V European Conference on Computational Fluid Dynamics
ECCOMAS CFD 2010
J. C. F. Pereira and A. Sequeira (Eds)
Lisbon, Portugal,14-17 June 2010

HIGH ORDER DISCONTINUOUS GALERKIN SOLUTION OF 1D IDEAL MAGNETOHYDRODYNAMIC EQUATIONS

A. Nigro* [†], **C. De Bartolo**[†], **F. Bassi**[‡]

[†] Università della Calabria,
Dipartimento di Meccanica, Ponte P. Bucci cubo 44/C, 87036 Rende (CS), Italy
e-mail: anigro@unical.it, c.debartolo@unical.it
[‡]Università di Bergamo
Dipartimento di Ingegneria Industriale, Viale Marconi 5, 24044 Dalmine (BG), Italy
e-mail: francesco.bassi@unibg.it

Key words: Magnetohydrodynamics, Discontinuous Galerkin, Riemann solver, Shock-capturing

Abstract. *In this work we present the results of high order Discontinuous Galerkin (DG) solutions of the unsteady one-dimensional ideal magnetohydrodynamic (MHD) equations. The work focused on assessing a shock-capturing technique coupled with the high order DG space discretization of MHD problems with discontinuous solutions. The main goal of shock-capturing techniques for high order DG methods is to achieve an optimal balance between sharp resolution of discontinuities and control of numerical oscillations. The technique here employed explicitly adds an artificial diffusion term to the DG discretized equations. The artificial viscosity is variable within the elements and for high order approximation the technique allows to achieve sub-cell resolution of discontinuities. The behavior of the shock-capturing technique here presented has been assessed by computing several shock-tube problems, using different numerical flux functions and for increasingly higher degree of the polynomial approximations.*

1 INTRODUCTION

Discontinuous Galerkin (DG) methods[1-6] for the numerical solution of partial differential equations have received much attention in the last years because of a number of properties, which make them well suited for very diverse fields of applications. In fact DG methods are both accurate and flexible, allowing high accuracy on arbitrary unstructured grids without compromising stability. Moreover, most DG discretizations are very compact thus allowing an easy and efficient parallelization of codes. Such favorable characteristics are of interest also in the field of magnetohydrodynamics (MHD).

Nowadays MHD is playing an important role both in advanced engineering applications and in astrophysics research problems. MHD flows can be very complex and very often they can develop several types of discontinuities. MHD problems are thus ideal to assess accuracy and robustness properties of numerical methods.

In this work we present the results of several numerical experiments on unsteady one-dimensional flows, governed by the ideal MHD equations, aimed at testing the effectiveness of a shock-capturing technique, inspired by the paper of Jaffre et al.[7], that has been developed for the Euler and Navier-Stokes equations and is here extended to the MHD equations.

The shock-capturing term has the form of an artificial viscosity term explicitly added to the high order DG space discretization of the governing equations. The shock-capturing technique has been implemented in a 1D DG code and has been evaluated coupled with numerical flux functions resulting from the solution of Riemann problems using a non-linear solver[8,9] and the linear HLL[10] and Roe's[11] approximate solvers.

The DG space discretized ODE system of equations is integrated in time using a multi-stage Runge-Kutta explicit method[12]. For the sake of efficiency, time integration of the shock-capturing term requires some degree of "implicitness" in order to avoid a large time step reduction entailed by a fully explicit treatment of the artificial viscosity term.

The performance of the shock-capturing approach has ben tested by computing several shock-tube problems involving both *regular* and *non-regular* waves[13]. The first test-case was presented by Dai and Woodward[8] and consists of seven *regular* waves, including fast shocks, slow shocks, rotational and contact discontinuities. In the second test-case a switch-on fast shock, which is a limiting case of a fast shock, forms and develops. The third test-case is one of the special shock-tube problems proposed by Torrilhon[14] to highlight the existence of non-unique solutions for a special class of MHD Riemann problems. Here we have considered the *non-regular* solution which involves a compound wave[15,16] consisting of an over-compressive shock and an attached rarefaction wave. Finally the fourth test-case is used to evaluate the performance of the code for a high Mach number flow condition.

The test problems have been computed up to P^8 polynomial approximation and the numerical results have been compared with exact solutions, either computed by means of a *regular* wave Riemann solver or provided to us by Torrilhon for the third *non-regular* wave problem.

In the following of the paper the governing equations are presented in Section 2. Section 3 is devoted to the numerical solution, including the DG space discretization, the shock-capturing

technique, the numerical fluxes and the time integration. Numerical results are presented and discussed in Section 4. Conclusions are finally given in Section 5.

2 GOVERNING EQUATIONS

We consider the one-dimensional ideal magnetohydrodynamic equations in the conservative form,

$$\frac{\partial \mathbf{u}}{\partial t} + \frac{\partial \mathbf{F}}{\partial x} = 0. \tag{1}$$

The conservative variables $\mathbf{u}$ and the flux vector $\mathbf{F}$ are given by:

$$\mathbf{u} = \begin{pmatrix} \rho \\ \rho u \\ \rho v \\ \rho w \\ B_y \\ B_z \\ \rho E^* \end{pmatrix}, \quad \mathbf{F} = \begin{pmatrix} \rho u \\ \rho u^2 + p^* - B_x^2 \\ \rho u v - B_x B_y \\ \rho u w - B_x B_z \\ B_y u - B_x v \\ B_z u - B_x w \\ \rho u H^* - B_x (B_x u + B_y v + B_z w) \end{pmatrix}. \tag{2}$$

Here ρ is the fluid density, u, v and w are velocity components, B_x,B_y and B_z are magnetic field components, p^* is the magnetic pressure, E^* is the magnetic energy per unit mass and H^* is the magnetic enthalpy per unit mass. Magnetic pressure, energy and enthalpy are defined by:

$$p^* = p + \frac{\mathbf{B}^2}{2} \tag{3}$$

$$E^* = e + \frac{1}{2}\mathbf{v}^2 + \frac{\mathbf{B}^2}{2\rho} \tag{4}$$

$$H^* = E^* + \frac{p^*}{\rho}. \tag{5}$$

We refer to p as the hydrodynamic pressure and to e as the internal energy per unit mass. Assuming the fluid satisfies the equation of state of a perfect gas, the hydrodynamic pressure is given by $p = (\gamma - 1)\,\rho e$, where γ is the ratio of specific heats of the fluid, given by $\gamma = c_p/c_v$. Since we are working in one dimension, the divergence free condition of the magnetic field $\nabla \cdot \mathbf{B} = 0$ reduces to B_x= const.

The seven eigenvalues of the Jacobian matrix $\frac{\partial \mathbf{F}}{\partial \mathbf{u}}$, representing the characteristic velocities of eq. (1), written in an increasing order are:

$$u - c_f, u - c_a, u - c_s, u, u + c_s, u + c_a, u + c_f \tag{6}$$

with:

$$c_a^2 = b_x^2 \tag{7}$$

$$c_f^2 = \frac{1}{2}\left((a^*)^2 + \sqrt{(a^*)^4 - 4a^2 b_x^2}\right) \tag{8}$$

$$c_s^2 = \frac{1}{2}\left((a^*)^2 - \sqrt{(a^*)^4 - 4a^2 b_x^2}\right) \tag{9}$$

and:

$$\mathbf{b} = \frac{\mathbf{B}}{\sqrt{\rho}}, \qquad \mathbf{b} = (b_x, b_y, b_z)^t \tag{10}$$

$$(a^*)^2 = a^2 + \mathbf{b}^2, \qquad a^2 = \gamma \frac{p}{\rho} \tag{11}$$

The corresponding roots $c_a^{\pm}$,$c_s^{\pm}$ and $c_f^{\pm}$ define the right (+) left (-) rotation (Alfven), slow and fast magnetoacoustic velocities, respectively. Furthermore, u defines the entropy (contact) velocity. The system (1) is hyperbolic if the eigenvalues are real and distinct. However, since $c_s \leq c_a \leq c_f$ the eigenvalues may coincide in some limiting case and the system becomes non-strictly hyperbolic. In the hyperbolic case the solution of the Riemann problem for the MHD system is governed by seven waves. Each wave can be either continuous or discontinuous, depending on initial data, and it is associated with a characteristic velocity as follows,

$$u \pm c_f \;:\; \text{fast shock or rarefaction to the right/left} \tag{12}$$

$$u \pm c_a \;:\; \text{rotational discontinuity to the right/left} \tag{13}$$

$$u \pm c_s \;:\; \text{slow shock or rarefaction to the right/left} \tag{14}$$

$$u \;:\; \text{contact discontinuity.} \tag{15}$$

Through the shock fronts there exist jumps in all the variables. The rotational discontinuity produces the rotation of magnetic field and jumps in the transverse components of the flow velocity, while in the contact discontinuity the jumps interest only density, temperature and entropy. As suggested by Torrilhon these waves will be called *regular* waves in the following, to distinguishing them from other ones that may arise because of the non-hyperbolicity of the MHD equations and non-convexity of the flux function[15].

3 NUMERICAL SOLUTION

3.1 DG Space Discretization

Multiplying eq. (1) by a vector-valued test function $\mathbf{v}$ and integrating by parts, we obtain the weak formulation, with built in boundary condition treatment:

$$\int_\Omega \mathbf{v} \cdot \frac{\partial \mathbf{u}}{\partial t}\, \mathrm{d}\mathbf{x} - \int_\Omega \nabla \mathbf{v} \colon \mathbf{F}(\mathbf{u})\, \mathrm{d}\mathbf{x} + \int_{\partial\Omega} (\mathbf{v} \otimes \mathbf{n}) : \mathbf{F}(\mathbf{u}_b)\, \mathrm{d}s = 0 \qquad \forall \mathbf{v} \in H^1(\Omega) \tag{16}$$

where $\mathbf{u}_b$ is a boundary state, Ω is the domain with boundary $\partial\Omega$, and $\mathbf{n}$ is the unit outward normal vector. To discretize in space, we define $\mathbf{V}_h^\kappa$ to be the space of discontinuous vector-valued polynomials of degree κ on a subdivision T_h of the domain into non-overlapping elements such that $\Omega = \bigcup_{K \in T_h} K$. Thus, the solution and test function space is defined by

$$\mathbf{V}_h^\kappa = \left\{ \mathbf{v} \in L^2(\Omega) : \mathbf{v}\,|_K \in P_\kappa, K \in T_h \right\}, \tag{17}$$

where P_κ is the space of polynomial functions of degree at most κ. The discrete problem then takes the following form: find $\mathbf{u}_h \in \mathbf{V}_h^\kappa$ such that

$$\sum_{K\epsilon T_h} \left\{ \int_K \mathbf{v}_h \cdot \frac{\partial \mathbf{u}_h}{\partial t} \, \mathrm{d}\mathbf{x} - \int_K \nabla \mathbf{v}_h : \mathbf{F}\left(\mathbf{u}_h\right) \, \mathrm{d}\mathbf{x} \right.$$
$$\left. + \int_{\partial K \backslash \partial \Omega} \left(\mathbf{v}_h^- - \mathbf{v}_h^+\right) \cdot \mathbf{H}_i \left(\mathbf{u}_h^+, \mathbf{u}_h^-, \mathbf{n}^-\right) \, \mathrm{d}s + \int_{\partial K \cap \partial \Omega} \left(\mathbf{v}_h \otimes \mathbf{n}\right) : \mathbf{F}\left(\mathbf{u}_b\right) \, \mathrm{d}s \right\} = 0 \tag{18}$$

for all $\mathbf{v}_h \in \mathbf{V}_h^\kappa$, where $\mathbf{H}_i \left(\mathbf{u}_h^+, \mathbf{u}_h^-, \mathbf{n}\right)$ is a numerical flux function defined on interior faces. $\mathbf{H}_i$ takes into account the possible discontinuities of $\mathbf{u}_h$ at element interfaces. On interior edges $\partial K \backslash \partial \Omega$, $\mathbf{H}_i$ depends on the elements interior state $\mathbf{u}_h^+$ and on the neighbouring elements state $\mathbf{u}_h^-$. On boundary edges $\partial K \cap \partial \Omega$, $\mathbf{u}_b$ is computed by combining the prescribed boundary data with the Riemann invariants associated to outgoing characteristic lines.

3.2 Shock-capturing

The shock-capturing approach consists of adding to the DG discretized equations an artificial viscosity term that aims at controlling the high-order modes of the numerical solution within elements while preserving as much as possible the spatial resolution of discontinuities. The shock-capturing term is local and active in every element, but the amount of artificial viscosity is proportional to the (inviscid) residual of the DG space discretization and thus it is almost negligible except than at locations of flow discontinuities. The shock-capturing term added to eq. (18) reads

$$\sum_{K\epsilon T_h} \int_K \epsilon \left(\mathbf{u}_h^\pm, \mathbf{u}_h\right) \left(\nabla \mathbf{u}_h \cdot \mathbf{b}\right) \left(\nabla \mathbf{v}_h \cdot \mathbf{b}\right) \mathrm{d}\mathbf{x}, \tag{19}$$

with the ϵ coefficient and the pressure gradient unit vector defined by

$$\epsilon \left(\mathbf{u}_h^\pm, \mathbf{u}_h\right) = C h_K^2 \frac{\left|s_p \left(\mathbf{u}_h^\pm, \mathbf{u}_h\right)\right| + \left|d_p \left(\mathbf{u}_h\right)\right|}{p_{(\mathbf{u}_h)}} f_p \left(\mathbf{u}_h\right), \quad \mathbf{b}\left(\mathbf{u}_h\right) = \frac{\nabla p \left(\mathbf{u}_h\right)}{\left|\nabla p \left(\mathbf{u}_h\right)\right| + \varepsilon}, \tag{20}$$

and

$$s_p \left(\mathbf{u}_h^\pm, \mathbf{u}_h\right) = \sum_i \frac{\partial p \left(\mathbf{u}_h\right)}{\partial \mathbf{u}_h^i} s_i \left(\mathbf{u}_h^\pm\right), \quad d_p \left(\mathbf{u}_h\right) = \sum_i \frac{\partial p \left(\mathbf{u}_h\right)}{\partial \mathbf{u}_h^i} \left(\nabla \cdot \mathbf{F}\left(\mathbf{u}_h\right)\right)_i. \tag{21}$$

The components s_i of the function $\mathbf{s}$ defined by the solution of the problem

$$\int_K v_h^i s_i \left(\mathbf{u}_h^\pm\right) \mathrm{d}\mathbf{x} = \int_{\partial K} v_h^i \left(\mathbf{H}_i \left(\mathbf{u}_h^+, \mathbf{u}_h^-, \mathbf{n}^-\right) - \mathbf{F}\left(\mathbf{u}_h\right) \cdot \mathbf{n}^-\right)_i \mathrm{d}s. \tag{22}$$

are actually the interface jumps between the numerical and internal inviscid flux components in normal direction. The further factor $f_p \left(\mathbf{u}_h\right)$ in eq. (20) is a pressure sensor defined by

$$f_p \left(\mathbf{u}_h\right) = \frac{\left|\nabla p \left(\mathbf{u}_h\right)\right|}{p \left(\mathbf{u}_h\right)} \left(\frac{h_K}{\kappa}\right), \tag{23}$$

which improves resolution of contact and rotational discontinuities. The scaling of the dimension h_K of the element K with degree of polynomial approximation, allows to tune the amount of added artificial viscosity for different polynomial degrees using a single value of the user-defined parameter C ($C = 0.05$ in all the following computations).

3.3 Numerical Fluxes

The numerical fluxes in eq. (18) have been computed by using three different Riemann solvers, namely a non-linear Riemann solver, that treats fast and slow rarefactions as "rarefaction shocks"[8], and the Roe[11] and HLL[10] approximate solvers. Exact solutions used in the following comparisons have been computed by means of an exact Riemann solver[8,9,17] in the case of *regular* wave solutions. The exact solution of the problem involving a compound wave has been provided to us by Torrilhon[14]. The three Riemann solvers employed for the evaluation of the numerical fluxes have been selected as representative of the solvers commonly used in the field of MHD. Moreover, this allowed to asses the behavior of the proposed shock-capturing scheme coupled to different numerical flux functions.

3.4 Time Integration

The DG space discretized eq. (18), including the shock-capturing term of eq. (19), results in the following system of equations

$$\mathbf{M}\left(\mathbf{U}\right)\frac{\mathrm{d}\mathbf{U}}{\mathrm{d}t} + \mathbf{R}\left(\mathbf{U}\right) + \mathbf{D}\left(\mathbf{U}\right)\mathbf{U} = 0, \tag{24}$$

where $\mathbf{U}$ and $\mathbf{R}$ are the vectors of solution degrees of freedom and of inviscid residuals. Using orthonormal basis functions for the polynomial approximation of the conservative variables of the governing equations, the mass matrix $\mathbf{M}\left(\mathbf{U}\right)$ simply reduces to the identity matrix. Notice that the discretized shock-capturing term has been written as the product of a block diagonal matrix $\mathbf{D}\left(\mathbf{U}\right)$ times the vector of solution DOFs. Each block of $\mathbf{D}$ couples the degrees of freedom of the components of $\mathbf{u}$ and within one element such blocks are equal to each other. The shock-capturing term is a diffusion-like term, typically subject to wild variations even within one element and that can attain large values in very few elements of the computational grid. Seeking to avoid any further time step restriction in the explicit time integration scheme, it is advisable to employ some degree of "implicitness"for the time integration of this term. For this purpose, eq. (24) is rewritten as

$$\mathbf{M}\left(\mathbf{U}\right)\frac{\mathrm{d}\mathbf{U}}{\mathrm{d}t} + \mathbf{R}\left(\mathbf{U}\right) + \mathbf{D}\left(\mathbf{U}\right)\left(\mathbf{U} + \mathrm{d}\mathbf{U}\right) = 0, \tag{25}$$

and this leads to

$$\frac{\mathrm{d}\mathbf{U}}{\mathrm{d}t} + \tilde{\mathbf{R}}\left(\mathbf{U}\right) = 0, \tag{26}$$

where

$$\tilde{\mathbf{R}}\left(\mathbf{U}\right) = \left[\mathbf{M}\left(\mathbf{U}\right) + \mathbf{D}\left(\mathbf{U}\right)\,\mathrm{d}t\right]^{-1}\left(\mathbf{R}\left(\mathbf{U}\right) + \mathbf{D}\left(\mathbf{U}\right)\mathbf{U}\right). \tag{27}$$

Solution of system (26) is advanced in time by means of the following s-stage SSP Runge-Kutta scheme[12],

$$\begin{aligned}
&\mathbf{U}^{(0)} = \mathbf{U}^n, \\
&\mathbf{U}^{(i)} = \mathbf{U}^{(0)} - \Delta t \sum_{k=0}^{i-1} c_{i,k} \tilde{\mathbf{R}}\left(\mathbf{U}^{(k)}\right) \qquad i = 1, 2, ..., s, \\
&\mathbf{U}^{n+1} = \mathbf{U}^{(s)},
\end{aligned} \tag{28}$$

where i is the stage counter and $c_{i,k}$ are the coefficients of the ith stage. We observe that the $c_{i,k}$ coefficients are related to the usual $a_{i,k}$ and b_k Butcher coefficients as follows

$$\begin{aligned}
a_{i,k} &= c_{i-1,k-1} \qquad k = 1, ..., i-1; \quad i = 2, ..., s, \\
b_k &= c_{s,k-1} \qquad k = 1, ..., s.
\end{aligned} \tag{29}$$

For equally spaced grid points, the time step Δt is computed by considering the classical CFL stability condition entailed by the TVD Runge-Kutta schemes, i.e. $CFL = 1/(2\kappa + 1)$. Using SSP Runge-Kutta schemes with more stages for a given order of temporal discretization it is possible to slightly improve the efficiency of the time integration.

4 RESULTS

In MHD the solution of the Riemann problem admits not only *regular* shocks and rarefactions but also switch-on fast shocks, switch-on slow rarefactions, switch-off slow shocks, switch-off fast rarefactions. Furthermore, it is possible to obtain over-compressive shocks due to the non-strict hyperbolicity of the MHD equations and non-convexity of the flux function[15]. This means that the wave speeds of two different structures may coincide and that compound structures consisting of an over-compressive shock and an attached rarefaction wave may arise. In this respect, we remind that the non-linear Riemann solver implemented in the DG cannot reproduce compound waves as it has been implemented for selecting *regular* waves only.

We present the performance of the technique for the control of oscillations by computing several shock-tube problems. Table 1 summarizes the test cases considered for this purpose. The TC1 test case is the Riemann problem designed by Dai and Woodward[8] to cover the entire range of MHD *regular* wave structures. To test the performance of the proposed shock-capturing approach in a limiting case of the fast shock and in the case of *non-regular* waves, we will show the numerical solutions for Riemann problems containing a switch-on fast shock (TC2) and a compound structure (TC3). Finally, the TC4 Riemann problem is used to evaluate the code for an high Mach number flow. For each test-case of table 1 we solve the one-dimensional MHD equations in the x-direction for $x \in [0, 1]$ with 200 equally spaced grid points using P_3, P_5, P_8 polynomial approximations.

Test-Case	ρ	p	u	v	w	B_y	B_z	B_x	γ	t
TC1-L	1.08	0.95	1.2	0.01	0.5	$3.6/\sqrt{4\pi}$	$2/\sqrt{4\pi}$	$2/\sqrt{4\pi}$	$5/3$	0.2
TC1-R	1	1	0	0	0	$4/\sqrt{4\pi}$	$2/\sqrt{4\pi}$			
TC2-L	1	1	0	0	0	1	0	1	$5/3$	0.15
TC2-R	0.2	0.1	0	0	0	0.0001	0			
TC3-L	1	1	0	0	0	1	0	1	$5/3$	0.05
TC3-R	0.2	0.2	0	0	0	$\cos\pi$	$\sin\pi$			
TC4-L	1	1000	0	0	0	1	0	0	2	0.006
TC4-R	0.125	0.1	0	0	0	-1	0			

Table 1: One-dimensional ideal MHD test cases.

The TC1 test case presented in the following has been investigated in grater detail in order to highlight the behavior of the proposed shock-capturing technique for MHD *regular* wave solutions. This initial-value problem involves seven discontinuities: a left-going fast shock, a left-going rotational discontinuity, a left-going slow shock, a contact discontinuity, a right-going slow shock, a right-going rotational discontinuity and a right-going fast shock.

For this test case, the figure 1 shows the numerical solution obtained with the various Riemann solvers using P_0 elements. As expected, the Roe scheme gives results very similar to that of the Godunov scheme, whereas the HLL numerical flux provides poor solution of the slow shock and of the contact discontinuity.

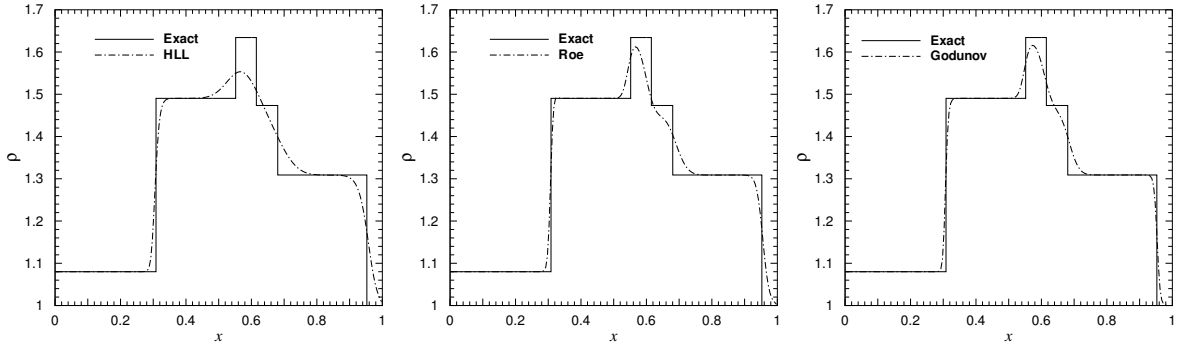

Figure 1: TC1 shock-tube problem for P_0 polynomial approximation, 200 elements. Exact solution of density (solid line) versus approximate solution (solid circle) computed by the HLL solver (left), the Roe solver (middle) and the Godunov solver (right).

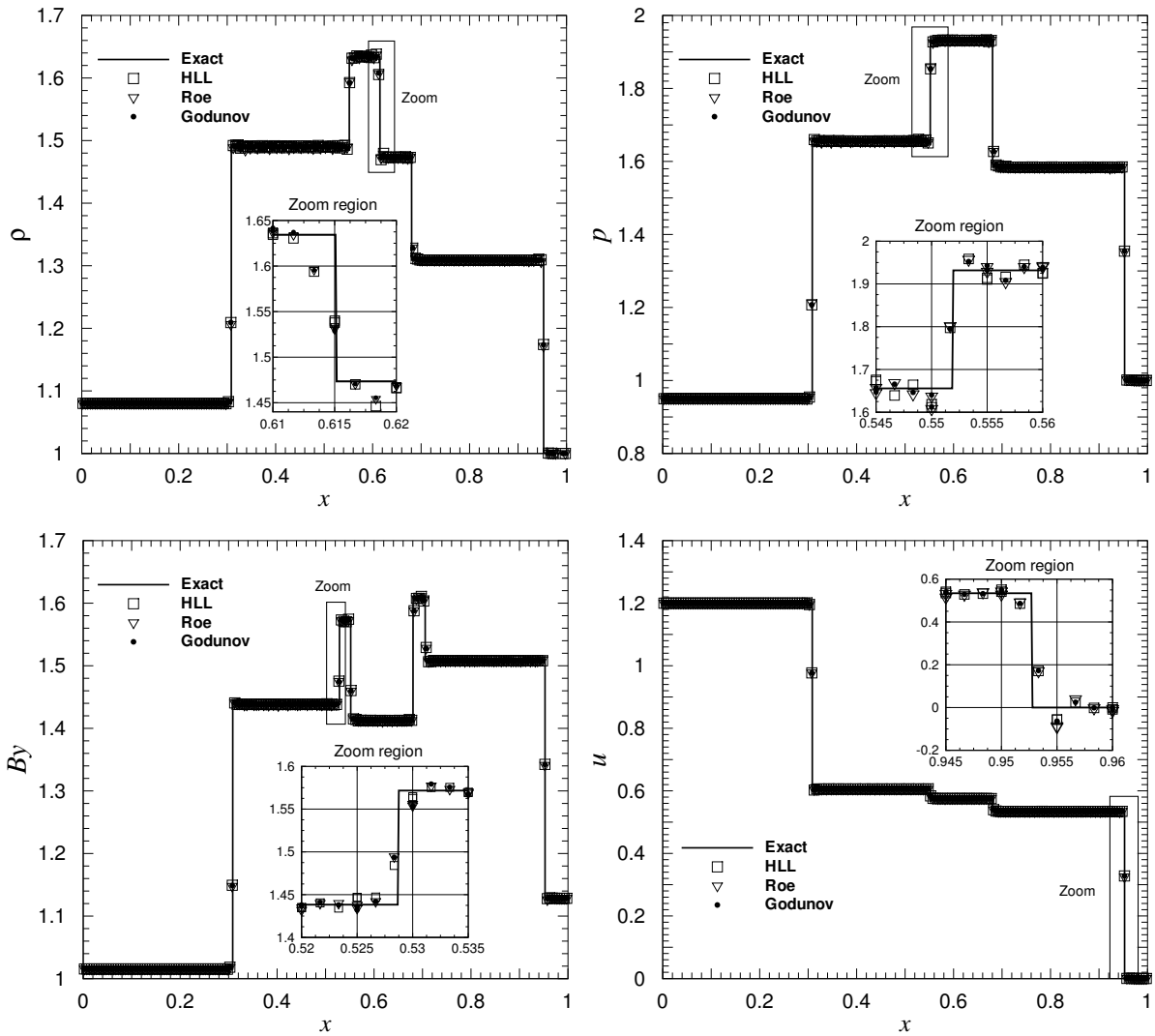

Figure 2: TC1 shock-tube problem for P_3 polynomial approximation, 200 elements. Density (top left), hydrodynamic pressure (top right), y-component of the magnetic field (bottom left) and x-component of the velocity (bottom right). Exact solution (solid line) versus approximate solution computed by the HLL solver (open square), the Roe solver (open triangle) and the Godunov solver (solid circle). In the plots average values within elements are shown. In the zoomed regions 4 plotting points for each element are shown.

Figure 2 shows that the P_3 average solutions obtained using different Riemann solvers are very close to each other and differences become even smaller raising the polynomial degree. We also observe that all the Riemann solvers are able to capture the discontinuity within one element.

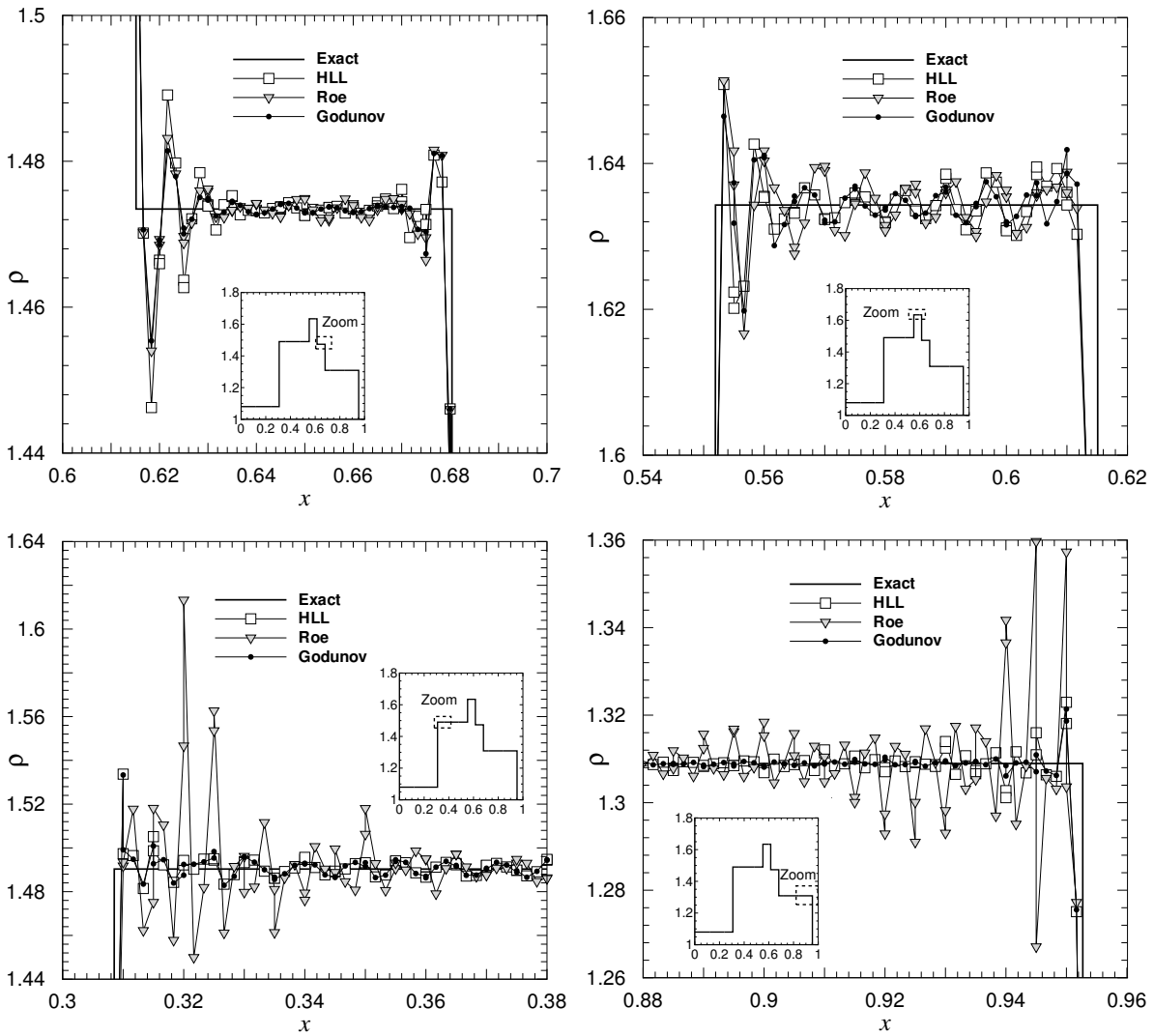

Figure 3: TC1 shock-tube problem for P_3 polynomial approximation, 200 elements. Post-shock oscillations of density. Exact solution (solid line) versus approximate solution computed by the HLL solver (white square), the Roe solver (gray triangle) and the Godunov solver (black circle). In the plots 4 plotting points for each element are shown.

Unlike the averaged distribution of figure 2 the plots of the polynomial representation of the density show some degree of oscillations in the flat regions away from discontinuities, as shown in figure 3. Such oscillations are relatively small for the HLL and Godunov schemes, whilst the Roe solver exhibits significant overshoots, undershoots and post-shock oscillations. In all cases the post-shock oscillations reduce moving away from the shock.

The next two figures compare solutions of the TC1 test case for increasingly higher degrees of polynomial approximation and using the HLL numerical flux.

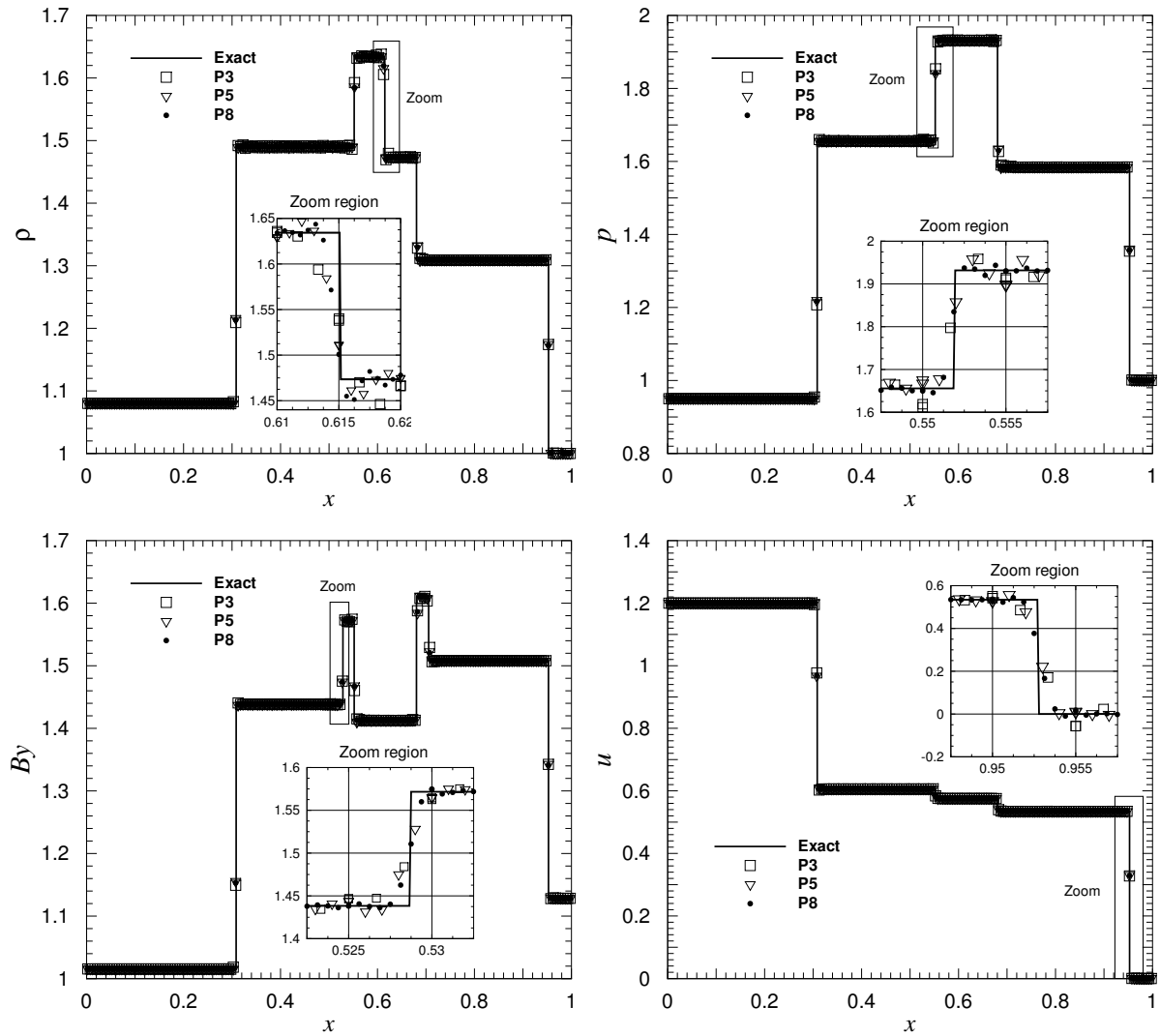

Figure 4: TC1 shock-tube problem, 200 elements. Density (top left), hydrodynamic pressure (top right), y-component of the magnetic field (bottom left) and x-component of the velocity (bottom right). Exact solution (solid line) versus P_3 (open square), P_5 (open triangle) and P_8 (solid circle) solutions computed by the HLL solver. In the plots average values within elements are shown. In the zoomed regions $\kappa + 1$ plotting points for each P_κ element are shown.

Figures 4 and 5 show that the resolution of the discontinuities improves and the post-shock oscillations reduce raising the degree of polynomial approximation.

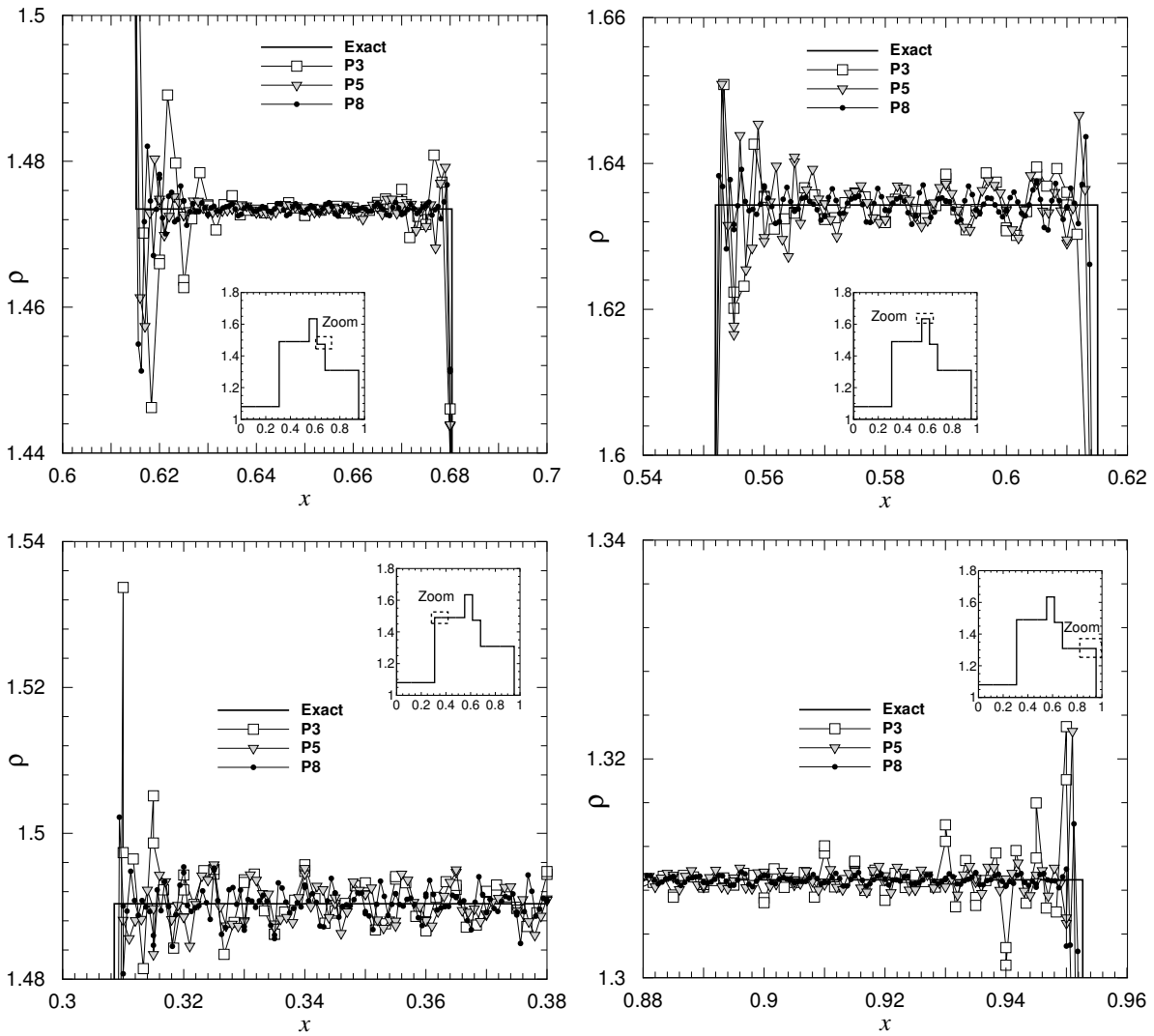

Figure 5: TC1 shock-tube problem, 200 elements. Post-shock oscillations of density. Exact solution (solid line) versus P_3 (white square), P_5 (gray triangle) and P_8 (black circle) solutions computed by the HLL solver. In the plots $\kappa + 1$ plotting points for each P_κ element are shown.

Some insight about the behavior of the artificial viscosity term can be gained by looking at the magnitude of the shock-capturing coefficient for a discontinuity moving through one element. Figures 6 and 7 show seven successive snapshots of the TC1 fast and slow right-going shocks while the shock front approaches and passes through one element of the grid. These figures highlight the local behavior of the artificial viscosity coefficient, which is activated just around the front of the shocks. On the other hand, for contact and rotational discontinuities, for which the pressure is continuous, the artificial viscosity is negligible, as shown in figure 8.

Figure 9 shows the numerical solutions of the other test-cases reported in table 1. The TC2 test-case (top row) involves a so called switch-on fast shock. This shock-tube problem consists of a left-going fast rarefaction, a left-going slow rarefaction, a contact discontinuity, a right-going slow shock and a right-going switch-on fast shock which turns on the magnetic field in the post-shock region. The zoomed regions show that this wave structure is well captured by the DG solution within one element with a very good control of oscillations. The TC3 test-case (middle row) shows the formation of a so-called compound wave. This shock-tube problem consists of a left-going fast rarefaction, a left-going compound, a contact discontinuity, a right-going slow shock and a right-going fast rarefaction. In this case the DG code selects the *non-regular* solution and the compound wave appears to be well resolved. The density exhibits low overshoots and post-shock oscillations which are almost negligible for the y-component of the magnetic field. The TC4 test-case (bottom row) is characterized by a strong expansion that produced an high Mach number flow. This shock-tube problem involves a left-going fast rarefaction, a tangential discontinuity, and a right-going fast shock. We note that the fast shock is resolved within one element and the tangential discontinuity is approximated within a couple of elements. The zoomed regions display around the head of the left-moving rarefaction wave the numerical solution of the density and of the y-component of the magnetic field.

5 CONCLUSIONS

We have presented a shock-capturing technique coupled with the high order DG solution of MHD problems with discontinuities. The performance of the proposed approach has been assessed by computing fourth-, sixth- and ninth-order simulations of several shock-tube problems involving both *regular* and *non-regular* waves. Overall, the numerical results show that all the considered wave structures are well reproduced. The shock-capturing technique proved to be effective using the Godunov and HLL numerical fluxes and slightly less satisfactory for the Roe's approximate Riemann solver, which exhibited significant overshoots, undershoots and post-shock oscillations. All the Riemann solvers are able to provide sub-cell resolution of discontinuities for higher order approximations.

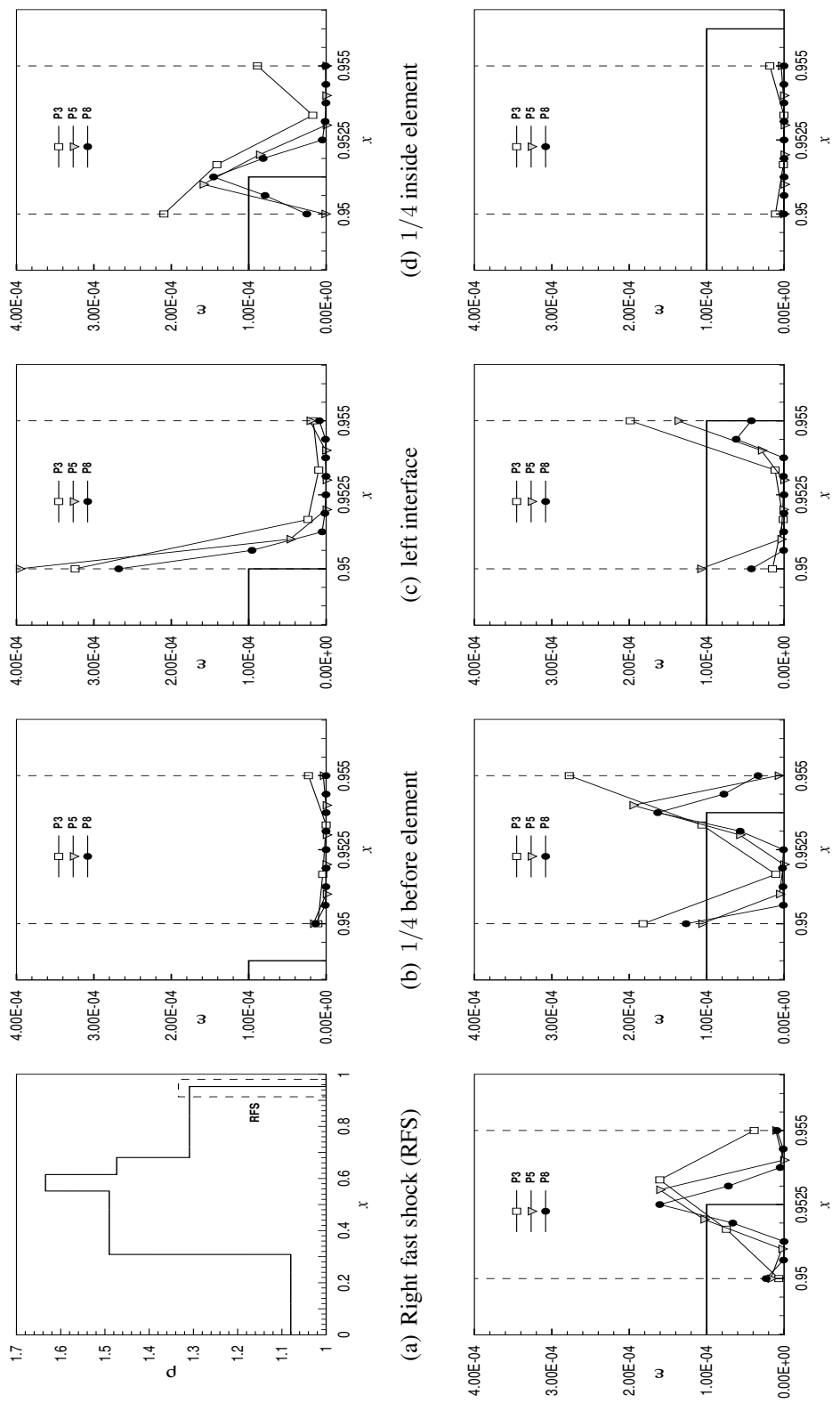

(a) Right fast shock (RFS) (b) $1/4$ before element (c) left interface (d) $1/4$ inside element

(e) $1/2$ inside element (f) $3/4$ inside element (g) right interface (h) $1/4$ after element

Figure 6: TC1 shock-tube problem, 200 elements. Local behavior of the ϵ coefficient when the right fast shock (solid line) moves (from left to right) across an element (dashed line). P^3 (white square), P^5 (gray triangle) and P^8 (black circle) solutions computed by the HLL solver. In the plots $\kappa + 1$ plotting points for each P_κ element are shown.

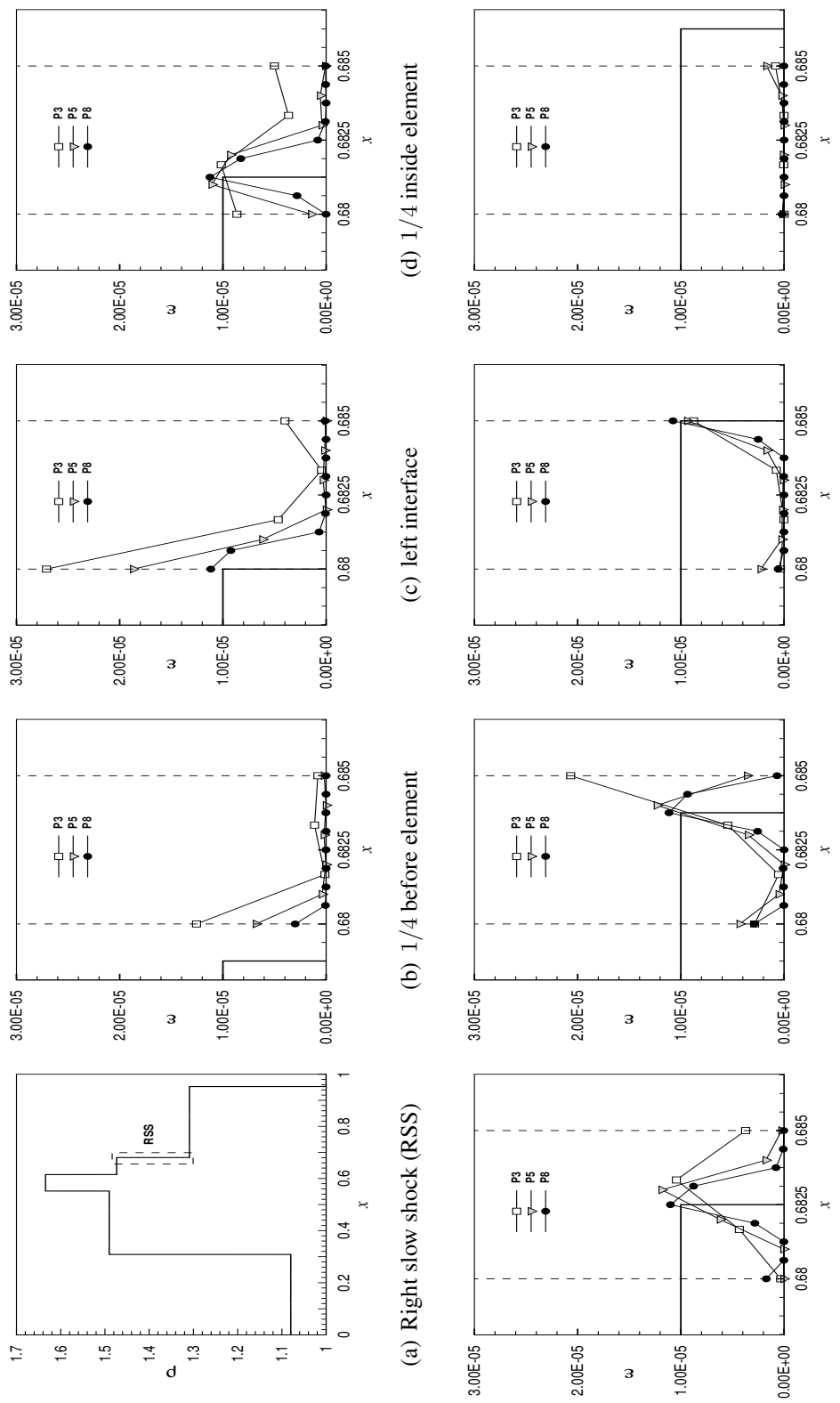

(a) Right slow shock (RSS) (b) $1/4$ before element (c) left interface (d) $1/4$ inside element

(e) $1/2$ inside element (f) $3/4$ inside element (g) right interface (h) $1/4$ after element

Figure 7: TC1 shock-tube problem, 200 elements. Local behavior of the ϵ coefficient when the right slow shock (solid line) moves (from left to right) across an element (dashed line). P^3 (white square), P^5 (gray triangle) and P^8 (black circle) solutions computed by the HLL solver. In the plots $\kappa + 1$ plotting points for each P_κ element are shown.

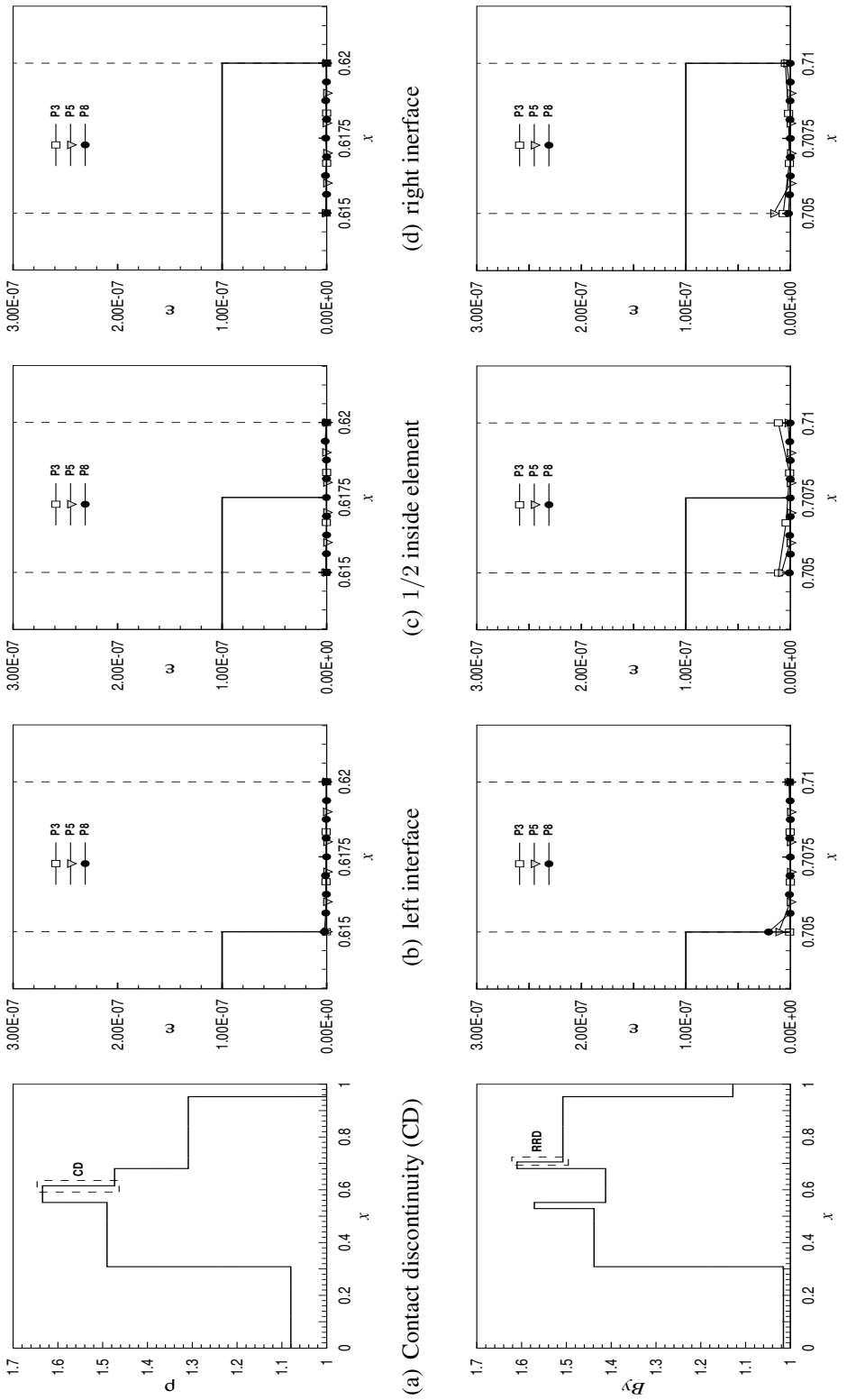

(a) Contact discontinuity (CD) (b) left interface (c) 1/2 inside element (d) right inerface

(e) Right rotational discontinuity (RDD) (f) left interface (g) 1/2 inside element (h) right interface

Figure 8: TC1 shock-tube problem, 200 elements. Local behavior of the ϵ coefficient when the contact discontinuity (a-d) and the right rotational discontinuity (e-h) (solid lines) move (from left to right) across an element (dashed line). P_3 (white square), P_5 (gray triangle) and P_8 (black circle) solutions computed by the HLL solver. In the plots $\kappa + 1$ plotting points for each P_κ element are shown.

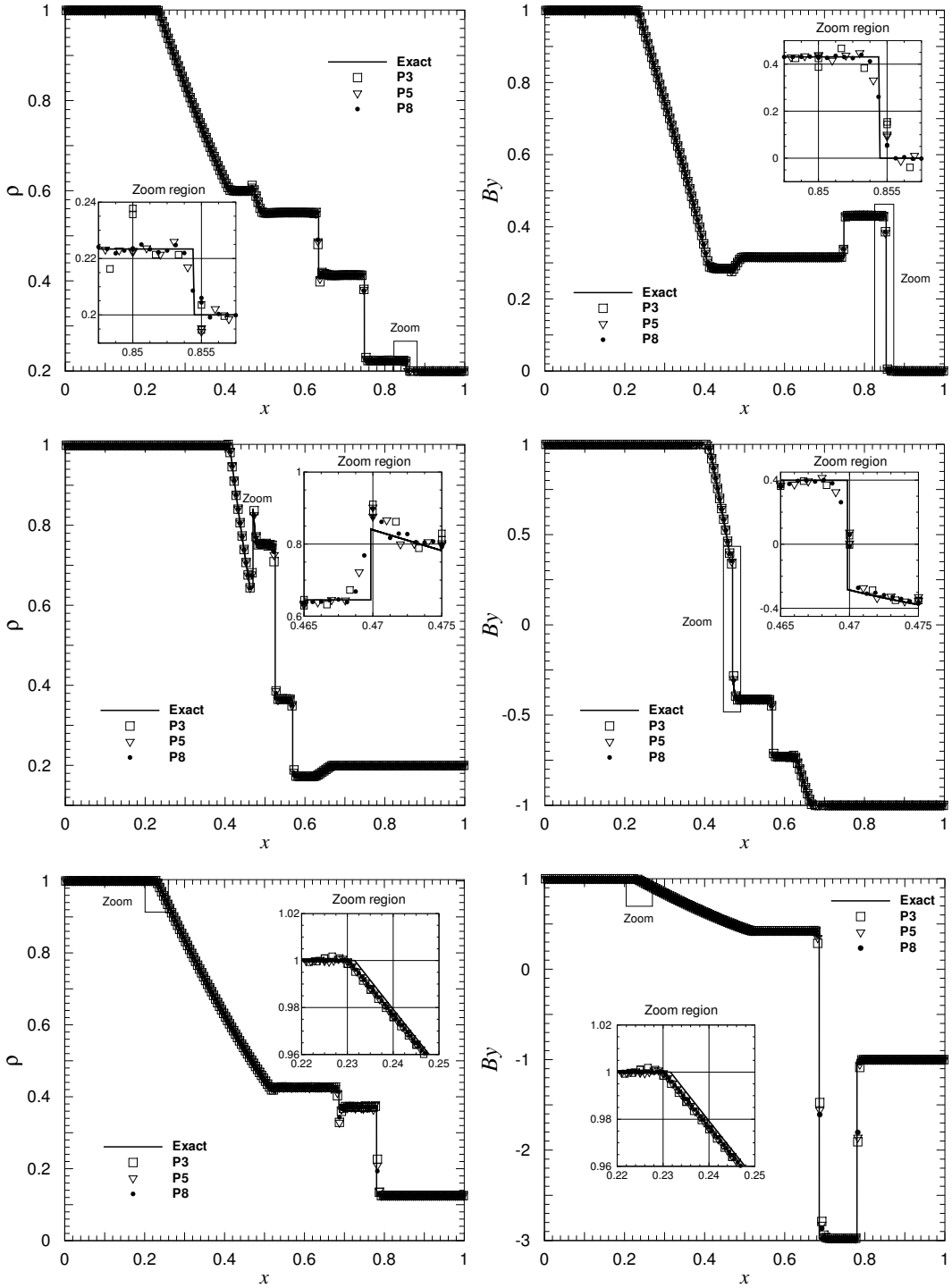

Figure 9: TC2 (top), TC3 (middle) and TC4 (bottom) shock-tube problems, 200 elements. Density (left) and y-component of the magnetic field (right). Exact solution (solid line) versus P_3 (open square), P_5 (open triangle) and P_8 (solid circle) solutions computed by the HLL solver. In the plots average values within elements are shown. In the zoomed regions $\kappa + 1$ plotting points for each P_κ element are shown.

ACKNOWLEDGEMENTS

We appreciate the helpful discussions with Dr. Bruno Giacomazzo during the implementation of the exact MHD Riemann solver. In addition, we thank Professor Manuel Torrilhon for providing the exact solutions of special MHD Riemann problems and for his insightful comments on *non-regular* wave solutions.

REFERENCES

[1] B. Cockburn, G. E. Karniadakis and C.-W. Shu, Discontinuous Galerkin methods: theory, computation, and applications, B. Cockburn, G. E. Karniadakis and C.-W. Shu (eds.), *Berlin: Springer* (2000).

[2] F. Bassi and S. Rebay, A high-order accurate discontinuous finite element method for the numerical solution of the compressible Navier-Stokes equations. *Journal of Computational Physics*, **131**, 267–279 (1997).

[3] F. Bassi, S. Rebay, G. Mariotti, S. Pedinotti and M. Savini, A High Order Accurate Discontinuous Finite Element Method for Inviscid and Viscous Turbomachinery Flows, *2nd European Conference on Turbomachinery-Fluid Dynamics and Thermodynamics*, 99–108 (1997).

[4] B. Cockburn and C.-W. Shu, The local discontinuous Galerkin method for time-dependent convection-diffusion systems. *SIAM J. Numer. Anal.*, **35**, 2440–2463 (1998).

[5] C. E. Baumann and J. T. Oden, A discontinuous hp finite element method for the Navier-Stokes equations, *10th International Conference on Finite Element in Fluids*, (1998).

[6] D. N. Arnold, F. Brezzi, B. Cockburn and D. Marini, Unified analysis of discontinuous Galerkin methods for elliptic problems, *SIAM J. Numer. Anal.*, **39**,1749–1779 (2002).

[7] J. Jaffre, C. Johnson and A. Szepessy, Convergence of the discontinuous Galerkin finite element method for hyperbolic conservation laws, *Math. Models Methods Appl. Sci.*, **5**, 367–386 (1995).

[8] W. Dai and P. R. Woodward, An Approximate Riemann Solver for Ideal Magnetohydrodynamics, *Journal of Computational Physics*, **111**, 354–372 (1994).

[9] D. Ryu and T.-W. Jones, Numerical Magnetohydrodynamics in Astrophysics: Algorithm and Tests for One-Dimensional Flow, *The Astrophysical Journal*, **442**, 228–258 (1995).

[10] A. Harten, P.-D. Lax and B. van Leer, On upstream differencing and Godunov-type schemes for hyperbolic conservation laws, *SIAM Rev.*, **25**, 35–61 (1983).

[11] P. Cargo and G. Gallice, Roe Matrices for ideal MHD and Systematic Construction of Roe Matrices for Systems of Conservation Laws, *Journal of Computational Physics*, **136**, 446-466 (1997).

[12] R. J. Spiteri and S.J. Ruuth, A new Class of Optimal High-Horder Strong-Stability-Preserving Time Discretization Methods, *Technical Report CS-2001-01*, Acadaia University, Wolfville, Nova Scotia, Canada, 2001.

[13] M. Torrilhon, Uniqueness conditions for Riemann problems of ideal magnetohydrodynamics, *Journal of Plasma Physics*, **69**, 253–276 (2003).

[14] M. Torrilhon, Non-uniform convergence of finite volume schemes for Riemann problems of ideal magnetohydrodynamics, *Journal of Plasma Physics*, **192**, 73–94 (2003).

[15] M. Brio and C.-C. Wu, An Upwind Differencing Scheme for the Equations of ideal Magnetohydrodynamics, *Journal of Computational Physics*, **75**, 400–422 (1988).

[16] A. Jeffrey and T. Taniuti, Non-linear Wave Propagation, *Academic Press, New York*, (1964).

[17] M. Torrilhon, Exact solver for Riemann problems of ideal magnetohydrodynamics, *Research report 2002-06*, Seminar for Applied Mathematics, ETH Zurich, (2002).